


Cite this: *RSC Adv.*, 2020, 10, 41511

Characteristics and mechanism of toluene removal by double dielectric barrier discharge combined with an $\text{Fe}_2\text{O}_3/\text{TiO}_2/\gamma\text{-Al}_2\text{O}_3$ catalyst

Rui Wang,^{id}*^{abc} Jiaze Ren,^{abc} Jiangyou Wu^{abc} and Lanlan Wu^{abc}

Removal of volatile organic compounds (VOCs) by non-thermal plasma technology produced by dielectric barrier discharge has become a hotspot due to its rapid reaction at room temperature, convenience without preheating and high removal efficiency of VOCs. Ways to improve the removal efficiency of mixed VOCs and the control of by-products in the discharge process are urgently needed. In view of the above shortcomings, the research progress of catalysts to improve the removal efficiency of VOCs by dielectric barrier discharge in recent years was reviewed; in this research, we conducted experiments on the removal efficiency of toluene under high flow rate experimental conditions (input voltage 10–70 V, mixed gas flow rate $1\text{ m}^3\text{ h}^{-1}$, inlet concentration 1000 mg m^{-3}). The research used $\gamma\text{-Al}_2\text{O}_3$, $\text{TiO}_2/\gamma\text{-Al}_2\text{O}_3$ and $\text{Fe}_2\text{O}_3/\text{TiO}_2/\gamma\text{-Al}_2\text{O}_3$ as catalysts in a reactor with a discharge gap of 6 mm, and a 99.7% removal efficiency of toluene was achieved when the SIE was 183.4 J L^{-1} . The added catalyst significantly reduced the concentration of by-products. At the same time, experiments with multiple catalysts to improve the removal efficiency and the performance of the discharge effect under different humidity levels were analyzed. The removal efficiency of toluene was optimized and recyclable, the formation of by-products was effectively suppressed when the catalysts in the reactor were $\text{Fe}_2\text{O}_3/\text{TiO}_2/\gamma\text{-Al}_2\text{O}_3$, $\text{TiO}_2/\gamma\text{-Al}_2\text{O}_3$ and $\gamma\text{-Al}_2\text{O}_3$, and the discharge length was 1 : 2 : 2.

Received 17th September 2020
Accepted 30th October 2020

DOI: 10.1039/d0ra07938c

rsc.li/rsc-advances

Introduction

Volatile organic compounds (VOCs), as the main components of air pollution, are produced in large quantities in the production processes of leather goods, inks, and decoration materials. Due to the health hazards of VOCs and their negative impact on the environment, the issue of effective removal of VOCs is urgent. Traditional methods such as physical adsorption, chemical absorption, condensation or biological methods are difficult to put into practical industrial application due to their cost and concentration limitations.^{1–5} Low-temperature plasma has become a research hotspot because of its high response rate to VOCs, the low cost of the processing technology and the convenience of opening and closing the experimental device.^{6–8}

Dielectric barrier discharge, a method for efficiently generating low-temperature plasma, involves applying an alternating voltage to two electrodes covered by an insulating medium to break down the working gas between the electrodes, accelerate free electrons, endow the gas with high energy and cause electron collapse.^{9–11}

The VOCs in the reactor are mainly degraded in two ways: in the first, the molecular structures of the VOCs themselves are destroyed by high-energy electrons and split into smaller particles, while in the second, high-energy electrons collide with gas molecules such as N_2 and O_2 . Free radicals and active ions with different degrees of reactivity are generated, and these products react with VOCs to achieve the effect of purifying the VOCs.¹²

In order to reduce the yield of by-products in the process of removing low-temperature plasma generated by dielectric barrier discharge to remove VOCs and improve the reaction efficiency, a catalyst is usually used for the cooperative reaction. Studies^{13–20} have shown that catalysts can effectively increase the reaction area, improve the removal efficiency of VOCs along with the selectivity of CO_2 , and reduce the formation of by-products.²¹

Materials and methods

Experimental setup

The experimental system consisted of a gas inlet system, DBD reactor (discharge length 200 mm, discharge distance 6 mm; the high-voltage electrode was stainless steel mesh, and the low-voltage electrode was quartz), pulse power supply (0–20 kV, 50% duty cycle, $f = 10\text{ kHz}$, $f_m = 200\text{ Hz}$, CTP-2000 K, pulse width $2.5 \times 10^{-3}\text{ s}$, China Jiangsu Suman Plasma Technology Co., Ltd.) and analysis system. Compressed air generated by an air compressor passes through the rotor flowmeter and enters the

*State Key Laboratory of Safety and Health for Metal Mines, Maanshan 243000, China.
E-mail: 564044540@qq.com

^bSinosteel Maanshan General Institute of Mining Research Co., Ltd., Maanshan 243000, China

^cHuawei National Engineering Research Center of efficient recycling for Metal Mineral Resources Co., Ltd., Maanshan 243000, China



mixing box in three ways. In the first way, air enters the cylinder containing toluene (I); in the second way, air enters the empty cylinder to control the air flow rate (I); in the third way, air enters the water-mixed gas bottle to control the humidity. Experimental gas enters the mixing box after the three-way gas merges and then enters the dielectric barrier discharge reactor after mixing evenly. The experimental system adjusts the gas flow rate, humidity and initial concentration of toluene through the flow meter and the manual valve of the air compressor to control the concentration of toluene at about 1000 mg m^{-3} and the relative humidity at about 30%. The inlet and outlet concentrations of toluene and CO_2 were measured by activated carbon adsorption/carbon analysis and gas chromatography, referring to the National Environmental Protection Standard of the People's Republic of China (HJ584-2010). The NO_x concentration was analyzed by a flue gas analyzer (KM950, Kane International Co. Ltd.). The O_3 concentration was measured by the iodometric method (Fig. 1).

The toluene removal efficiency was defined as

$$\eta = (C_0 - C)/C_0 \times 100\%.$$

The selectivity of CO_2 was defined as

$$S_{\text{CO}_2} = C_{\text{CO}_2}/7(C_0 - C).$$

Preparation of catalyst

Activation of $\gamma\text{-Al}_2\text{O}_3$: deionized water was used to clean the alumina pellets, the pellets were dried at 100°C for 3 h, and the temperature was raised to 550°C at 5°C per minute in a muffle furnace. After roasting for 3 h, the pellets were set aside.

Preparation of $\text{TiO}_2/\gamma\text{-Al}_2\text{O}_3$

TiO_2 powder was dispersed in 100 mL of deionized water containing 0.1% polyethylene glycol and ultrasonically dispersed at 30°C for 30 min; then, the activated $\gamma\text{-Al}_2\text{O}_3$ pellets were immersed in the catalyst dispersion for 10 min. The powder was removed and roasted in a muffle furnace at 150°C for 2 h.

Preparation of $\text{Fe}_2\text{O}_3/\text{TiO}_2/\gamma\text{-Al}_2\text{O}_3$

10 g of titanium dioxide powder was mixed with a certain amount of $\text{Fe}(\text{NO}_3)_3$ solution, stirred well and then ultrasonically dispersed for 10 min; after being kept open at 120°C for 4 h, the solution was evaporated and the powder was removed. 100 mL deionized water containing 0.1% polyethylene glycol was added; the mixture was stirred uniformly and ultrasonically dispersed for 30 minutes. The activated $\gamma\text{-Al}_2\text{O}_3$ was soaked in this mixture for 30 minutes, then calcinated in a muffle furnace at 150°C for 1 hour and calcinated under increasing temperature at a rate of 10°C every 15 minutes for 2 hours.

Measuring method of energy density

An error occurred in the power measurement caused by the action of the alternating electric field because the phase difference between the discharge voltage and current is difficult to measure. Therefore, in this study, we used the Lissajous method to determine the discharge power. The principle is to connect a measuring capacitor in series with the internal load of the power supply (its capacitance value C_M is known and is much larger than the equivalent capacitance of the reactor load); the circuit diagram is shown in Fig. 2.

At the same time, the voltage $U(t)$ applied to the load and the voltage $U_c(t)$ on the measuring capacitor were connected to the oscilloscope, and the relationship of the $U(t)-t$ curves, $U_c(t)-t$ curves and closed response U (the Lissajous curve of $t-U_c(t)$) is shown in Fig. 3. By integrating the Lissajous figure area, the discharge power of the reactor can be calculated by a formula. From this, the specific input energy of the DBD reactor can be calculated. The calculation formula is as follows:^{22,23}

$$P(\text{W}) = f_m \times \text{capacitance} \times S_{\text{lissajous}}$$

$$\text{SIE} (\text{J L}^{-1}) = \frac{60 \times P(\text{W})}{Q (\text{L min}^{-1})}$$

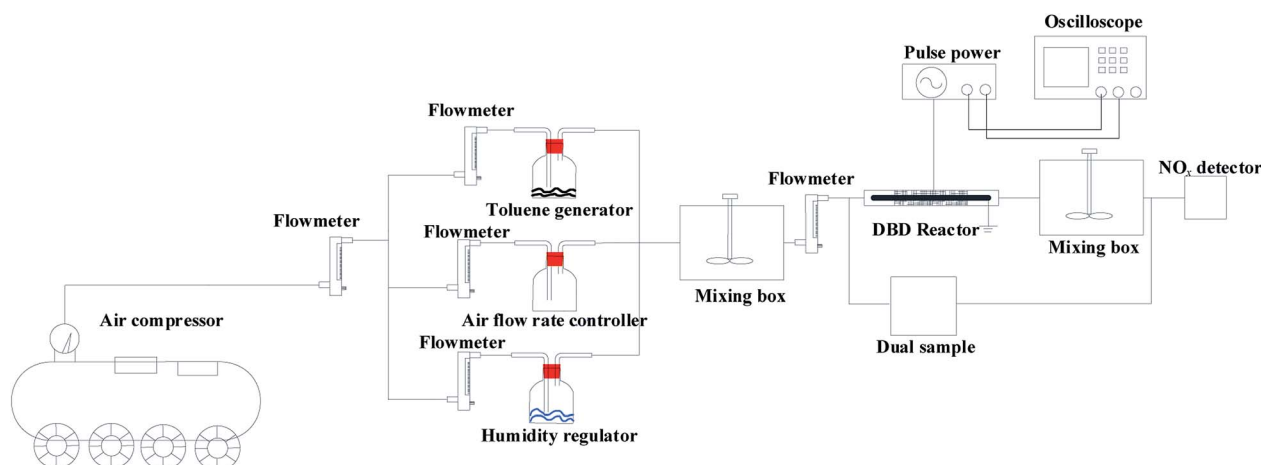


Fig. 1 Experimental system.



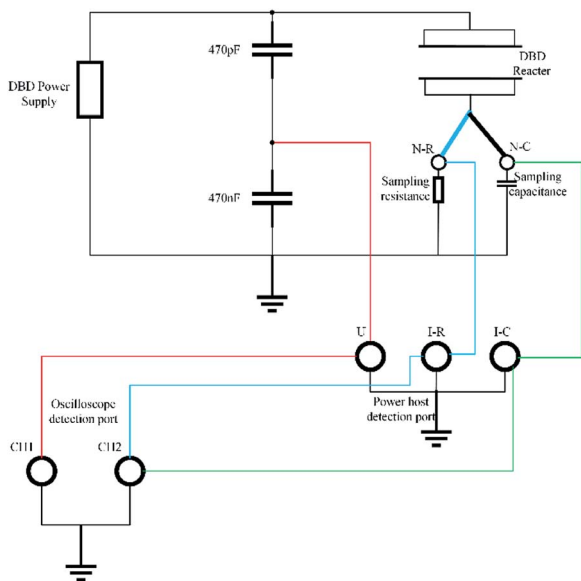


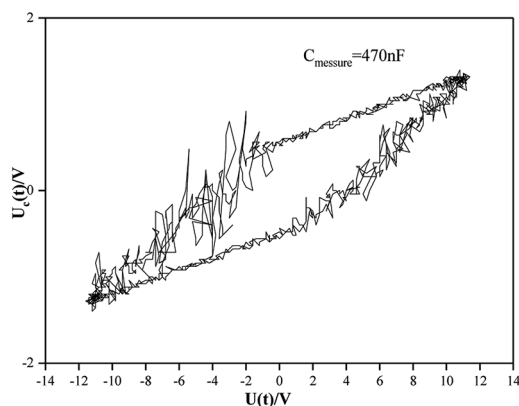
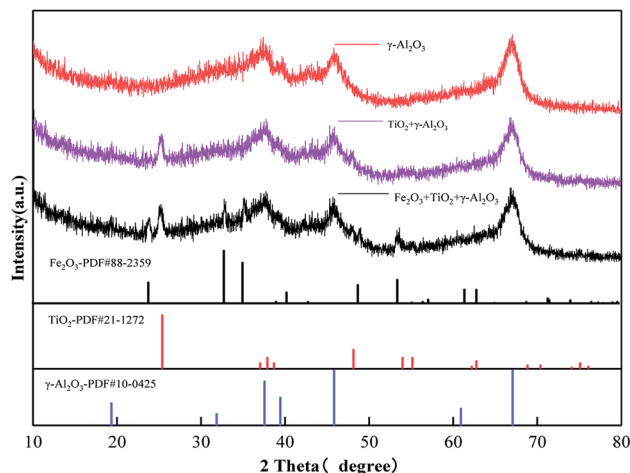
Fig. 2 Circuit diagram.

Results and discussion

Characterization of the catalysts Fe_2O_3 , TiO_2 , and $\gamma\text{-Al}_2\text{O}_3$

Fig. 4 shows the XRD patterns of $\gamma\text{-Al}_2\text{O}_3$ and other catalysts based on $\gamma\text{-Al}_2\text{O}_3$. As shown in Fig. 4, the diffraction peaks of Al_2O_3 appear at $2\theta = 19.45^\circ, 31.93^\circ, 37.63^\circ, 39.49^\circ, 45.86^\circ$, and 67.03° , which correspond well to PDF no 10-0425; this proves that the crystal form of alumina is $\gamma\text{-Al}_2\text{O}_3$.

After loading TiO_2 , the diffraction peaks appearing at $2\theta = 25.28^\circ, 37.8^\circ, 48.05^\circ, 62.69^\circ$, and 75.02° correspond well to the standard pd of anatase (PDF no 21-1272). After loading Fe_2O_3 , the diffraction peaks appearing at $2\theta = 23.85^\circ, 32.85^\circ, 35.08^\circ, 40.32^\circ, 48.82^\circ, 53.5^\circ$, and 61.53° correspond to hematite (PDF no 88-2359). However, the peak intensity corresponding to Fe_2O_3 (hematite, PDF number 88-2359) is low and has a slight deviation. This is because loading Fe on Al_2O_3 will shift the peak to a larger angle.²⁴ Due to the low loading and good spreading, the peak of Fe_2O_3 is not obvious in the XRD test results; however, the EDS test results (Fig. 5) show that sample 2 and sample 3 are successfully loaded with Ti and Fe.²⁵

Fig. 3 The relationship of $U_c(t)$.Fig. 4 XRD patterns of bare $\gamma\text{-Al}_2\text{O}_3$, $\text{TiO}_2/\gamma\text{-Al}_2\text{O}_3$ and $\text{Fe}_2\text{O}_3/\text{TiO}_2/\gamma\text{-Al}_2\text{O}_3$.

The SEM results (Fig. 6) also support this point of view: as shown in Fig. 6(a), the surface of the bare $\gamma\text{-Al}_2\text{O}_3$ is smooth; as shown in Fig. 6(b), TiO_2 (anatase) is loaded on the surface of $\gamma\text{-Al}_2\text{O}_3$ as small unevenly dispersed particles, showing an irregular morphology; in Fig. 6(c), the Fe_2O_3 hematite in the form of irregular flakes and blocks is loaded on the surface of $\text{TiO}_2/\gamma\text{-Al}_2\text{O}_3$. It can be seen that compared with small TiO_2 particles, larger flakes and massive particles appear on the surface of the catalyst. However, the surface of the catalyst still maintains an overall dense morphology, indicating that the loading of $\text{Fe}_2\text{O}_3/\text{TiO}_2$ does not change the basic structure of the catalyst carrier $\gamma\text{-Al}_2\text{O}_3$.

It can be seen from Fig. 7(a) that the xps spectra of O 1S of hematite, anatase and $\gamma\text{-Al}_2\text{O}_3$ can be fitted to three forms of peaks. The diffraction peak with a binding energy of 529.76 eV corresponds to the lattice oxygen (O_a) on the catalyst surface. The diffraction peak with a binding energy of 531.58 eV corresponds to the adsorbed oxygen (O_c) on the catalyst surface, and the diffraction peak with binding energy at 532.96 eV corresponds to the hydroxyl oxygen or oxygen in water (O_d) due to adsorption on the catalyst surface. Among them, adsorbed oxygen (O_c) accounts for a higher proportion, which can improve the catalytic activity of the catalyst and is beneficial to the oxidation process of VOCs. The diffraction peak binding energy in the xps spectrum of $\gamma\text{-Al}_2\text{O}_3$ is 74.41 eV, indicating that Al exists in the form of Al^{3+} . The XPS spectrum of Ti in the catalyst is shown in Fig. 7(c). The diffraction peaks of anatase at 458.35 eV and 463.98 eV correspond to Ti 2p_{3/2} and Ti 2p_{1/2}. This shows that Ti^{4+} exists on the catalyst surface. The XPS spectrum of Fe 2p in the catalyst is shown in Fig. 7(d). The diffraction peaks of hematite at 710.59 eV and 723.46 eV correspond to Fe 2p_{1/2} and Fe 2p_{3/2}, respectively, and the accompanying peaks are at 718.16 eV, indicating that hematite on the surface of the catalyst exists in the form of Fe^{3+} .²⁶ The diffraction peaks of the three elements of Al, Ti and Fe in the catalyst are all shifted to a certain extent compared to the standard XPS spectrum. Combined with XRD, it can be seen



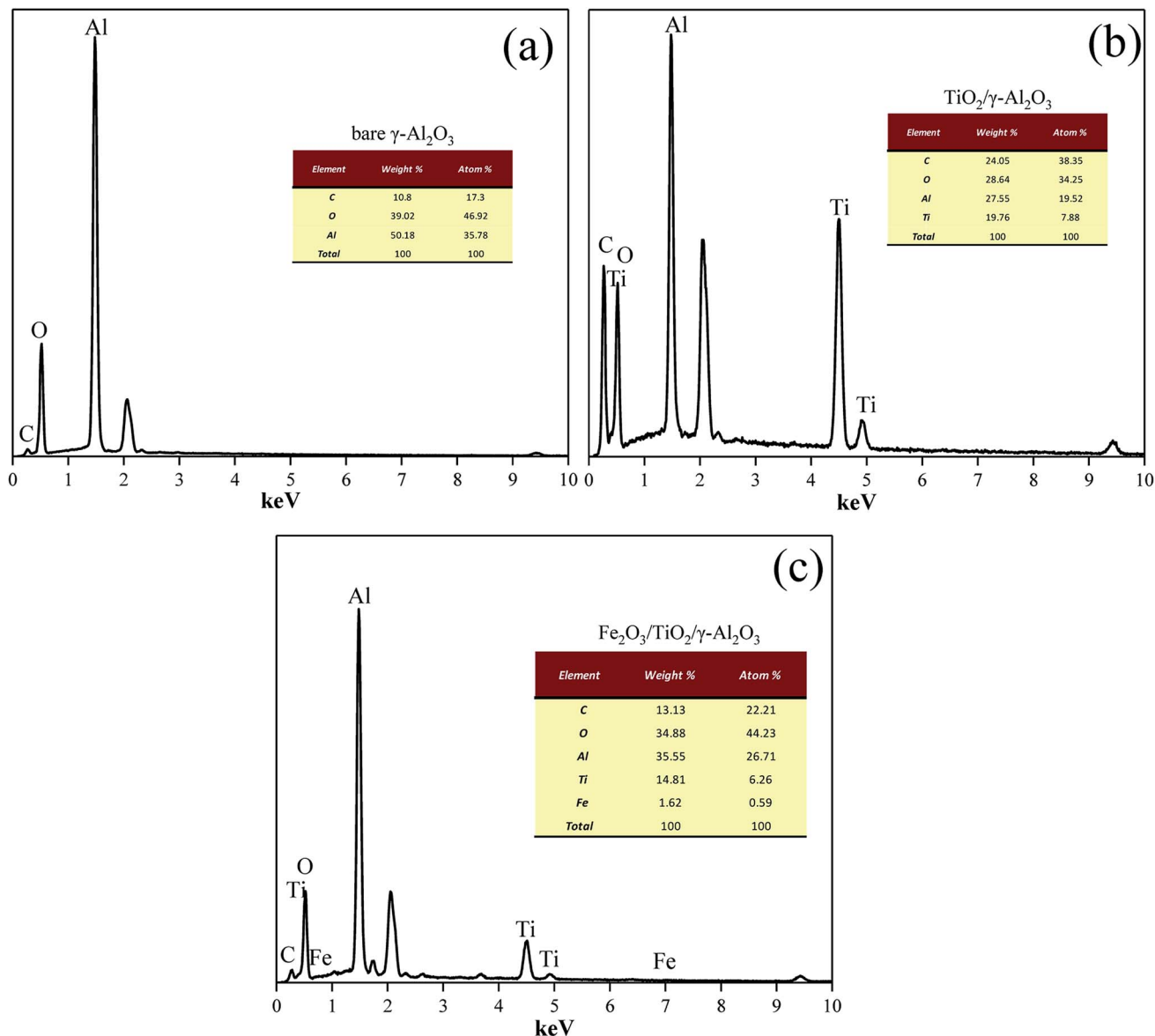


Fig. 5 EDS patterns of bare $\gamma\text{-Al}_2\text{O}_3$ (a), $\text{TiO}_2/\gamma\text{-Al}_2\text{O}_3$ (b) and $\text{Fe}_2\text{O}_3/\text{TiO}_2/\gamma\text{-Al}_2\text{O}_3$ (c).

that the interaction between $\gamma\text{-Al}_2\text{O}_3$, anatase and hematite in the catalyst changes the electron cloud density of the surface elements, which is beneficial to the catalytic oxidation of VOCs.²⁷

Influence of input voltage on output power and SIE

As shown in Fig. 8, the increase of the specific input energy (SIE, which is also called specific energy density) showed a trend of slow and then fast with increasing input voltage. After the input

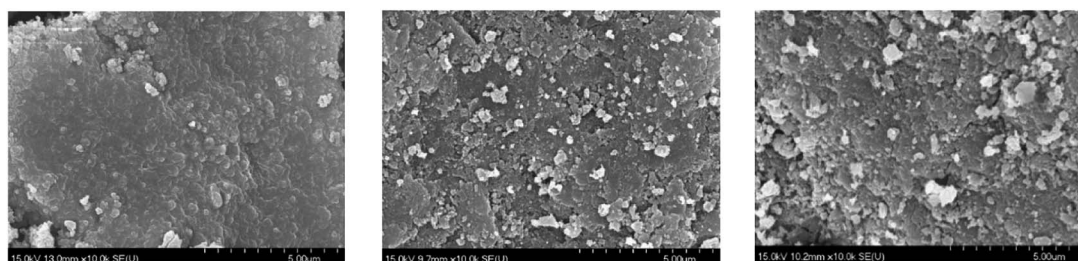


Fig. 6 SEM patterns of bare $\gamma\text{-Al}_2\text{O}_3$, $\text{TiO}_2/\gamma\text{-Al}_2\text{O}_3$ and $\text{Fe}_2\text{O}_3/\text{TiO}_2/\gamma\text{-Al}_2\text{O}_3$.



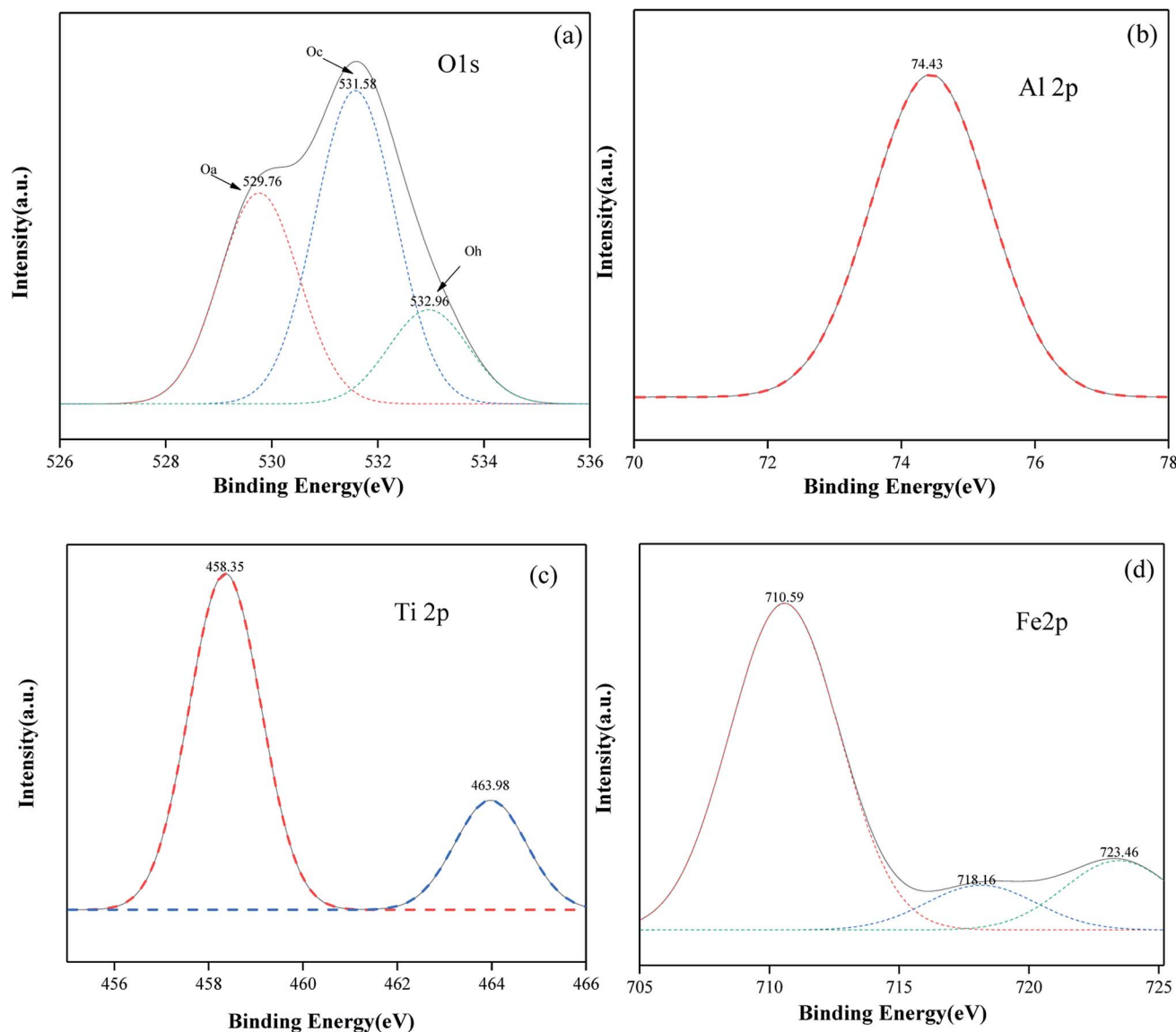


Fig. 7 XPS patterns of O (a), Al (b), Ti (c), and Fe (d) on the surface of $\text{Fe}_2\text{O}_3/\text{TiO}_2/\gamma\text{-Al}_2\text{O}_3$.

voltage was greater than 60 V, the growth rate gradually tended to be flat. The SIE values of the three curves represented by the reactor with catalyst added were significantly higher than the SIE value of the curve represented by a single DBD reactor because the addition of catalyst reduced the discharge gap, increased the peak voltage and ionized more high-energy particles. Therefore, the collision probability of high-energy particles and gas molecules in the dielectric barrier discharge process was improved, and the value of SIE increased.

Moreover, the power increased slowly when the input voltage was 10–30 V, and the trend grew faster when the input voltage was 30–60 V. The curve with the added catalyst was similar to the value of the power compared to the single DBD due to the addition of the catalyst, which increased the peak voltage. At the same time, the smaller discharge interval caused the current to decrease; therefore, there is not much difference in the power value.

Influence of SIE on the toluene removal efficiency and selectivity of CO_2

In the single DBD process, the removal efficiency of toluene and the selectivity of CO_2 were both low because the residence time of toluene gas in the DBD process was relatively short and it could not be completely degraded. As a result, it was difficult to generate CO_2 . The addition of the catalyst significantly improved the removal rate of toluene at various energy densities. The $\gamma\text{-Al}_2\text{O}_3$ catalysts loaded with TiO_2 and $\text{TiO}_2/\text{Fe}_2\text{O}_3$ increased the removal efficiency of toluene by 20.48% and 28.94% compared with a single DBD and the selectivity of CO_2 was increased by 32.55% and 35.85%, respectively. It can be seen from Fig. 9 that the removal rate of toluene by the reactor loaded with different catalysts improved with increasing SIE, which showed an increasing trend of fast and then slow. This is because with the increase of the applied electric field, more free

radicals were produced during the reaction, and the electrons produced had higher energy. These high-energy particles would accelerate the decomposition of toluene. However, the high-energy electrons and free radicals generated were sufficient to destroy the lower-energy chemical bonds in the pollutants as the energy density gradually increased, and the removal rate increased slowly as the energy density continued to increase because the generated electrons had higher energy and more radical groups decomposed chemical bonds and grouped with higher energy moieties, such as benzene rings. At the same time, the pollutants completely decomposed and oxidized the intermediate products generated during the reaction into CO_2 and H_2O . This change improved the selectivity of CO_2 ; however, it slowed the increase in the removal rate as well.

Under the same SIE, the removal rate of toluene by the reactor loaded with catalyst was higher than that of the ordinary DBD reactor, indicating that the presence of $\gamma\text{-Al}_2\text{O}_3$ pellets loaded with TiO_2 and Fe_2O_3 could effectively promote the degradation of organic matter. When the SIE was higher than 150 J L^{-1} , the difference in the removal rate was reduced because the energy was enough to destroy the structure of most toluene molecules without the help of an external catalyst. Therefore, the addition of the catalyst could improve the energy utilization rate to a certain extent and reduce the energy consumption during the DBD reaction process.

Influence of SIE on NO_x concentration

In the DBD process, electrons collided with background gas molecules such as O_2 and N_2 , generating ground and excited oxygen and nitrogen atoms. These oxygen atoms and nitrogen atoms would further react with O_2 and O_3 to produce NO and NO_2 . This study investigated the amount of NO_x produced by the DBD reactor and the catalyst-loaded reactor under different values of SIE. As shown in Fig. 10, the NO_x concentration gradually increased as the SIE increased because the higher SIE reflected the higher discharge energy in the reaction. The extra NO_x generated could not be reduced like O_3 , which decomposes

at high temperature, and could not be used as a reactant to promote the oxidation of toluene; therefore, the concentration of NO_x gradually increased.^{28,29}

The DBD reactor had the worst mineralization efficiency but the highest NO_x output. It was found that the excessive energy in the DBD reactor was consumed in the process of forming NO_x , which was an important reason for its low mineralization rate. Under the same value of SIE value, NO_x was generated due to the short reaction time between the active group and the toluene molecule, in which the toluene molecule could not be purified while the active group was consumed. After adding the catalyst, on the one hand, the pollutants and background gas molecules were adsorbed on the surface of the carrier, and the probability that the active groups on the carrier surface would react with the pollutant gas molecules and oxygen molecules was improved compared with N_2 molecules. On the other hand, the precursors of NO_x -active oxygen atoms and excited nitrogen molecules or nitrogen atoms were consumed on the surface of the catalyst, resulting in a decrease in the concentration of NO_x . Due to the above reasons, the reactor loaded with the catalyst had a higher energy utilization rate.

As shown in Fig. 10, the reactor loaded with $\gamma\text{-Al}_2\text{O}_3$ catalyst could control the production of NO_x well. When the surface of $\gamma\text{-Al}_2\text{O}_3$ was loaded with TiO_2 and Fe_2O_3 , the NO_x concentration of the two reactors was higher than that of the $\gamma\text{-Al}_2\text{O}_3$ reactor, and the total NO_x concentration of the two reactors was not much different.

Influence of SIE on O_3 concentration

The principle of the synergy between the DBD process and a heterogeneous catalyst is that the ultraviolet light and high-energy particles generated during the DBD discharge process can excite TiO_2 and generate hole-electron pairs. At the same time, $\gamma\text{-Al}_2\text{O}_3$ as the catalyst carrier plays a role in adsorbing pollutant molecules, while the addition of Fe_2O_3 also improves the catalytic activity. Under the action of the DBD electric field, the active material produced will react with the pollutant molecules adsorbed on the surface of the catalyst, and the holes

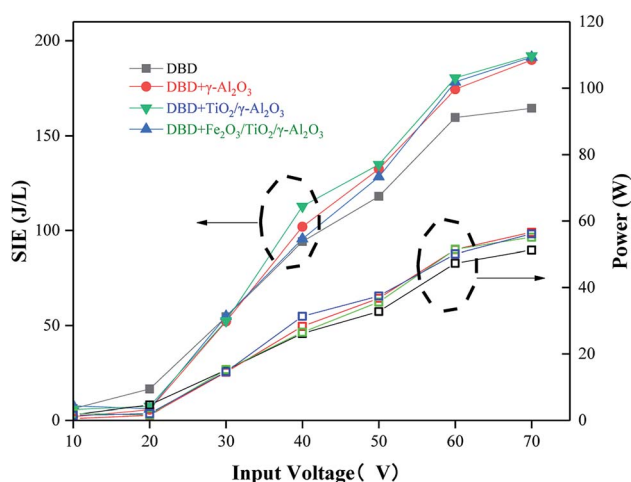


Fig. 8 The relationships between SIE and the change in output power with input voltage in different types of DBD reactors.

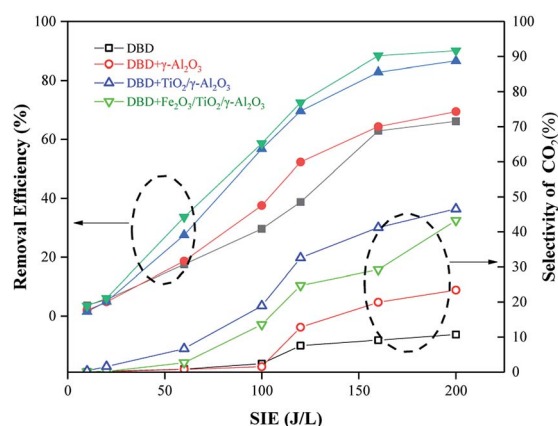


Fig. 9 The relationship between the removal efficiency and selectivity of CO_2 with SIE in different types of DBD reactors.



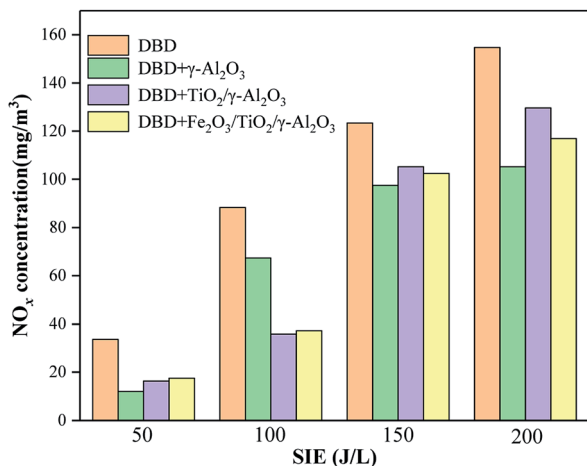


Fig. 10 The relationships between SIE and NO_x concentration in different types of DBD reactors.

will also directly oxidize the pollutant molecules or oxidize H₂O molecules to form \cdot OH. During the reaction process, ozone went through the following process: (1) the hole–electron pair generated after TiO₂ was excited had strong oxidizing properties, and a large amount of O₃ was generated; (2) during the DBD process, a large amount of O₃ was generated; (3) direct reactions with pollutant molecules on the catalyst surface occurred; (4) the pollutant molecules reacted with the precursors, which produced O₃ on the surface of the catalyst.

In the DBD reaction process, O₃ is an inevitable by-product. This study investigated the changes in the concentration of O₃ produced in the DBD process in different reactors under different values of SIE. As shown in Fig. 11, the amount of O₃ produced in all the DBD reactors showed an initial rapidly increasing trend and then slowly increased with increasing SIE because the increase of SIE would lead to an increase in the energy and in the number of higher-energy electrons inside the reactor. These higher-energy electrons could easily destroy the O=O bond, converting O₂ into O₃; meanwhile, more high-

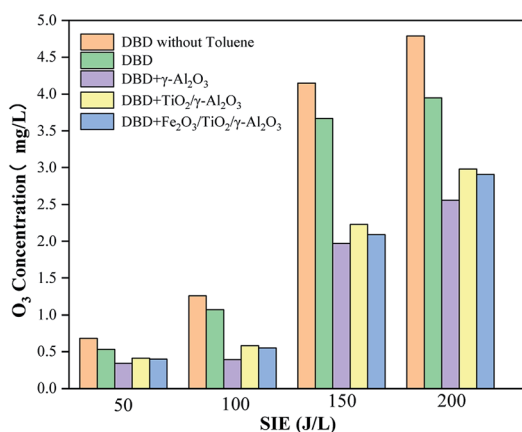


Fig. 11 The relationships between SIE and O₃ concentration in different types of DBD reactors.

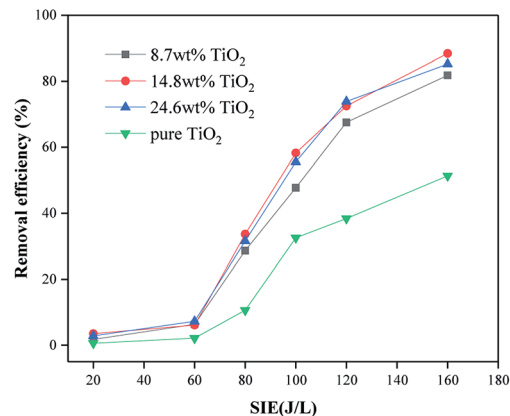


Fig. 12 Removal efficiencies of different TiO₂ catalytic reactors.

energy electrons and free radical groups were generated, and these high-energy electrons and free radical groups would decompose O₃ into O₂ when the energy density increased at the same time. O₃ was not only a byproduct but also an oxidant which could oxidize toluene and the intermediate products. The above reasons together led to an increase in ozone content.

When toluene was introduced, the O₃ concentration decreased. On the one hand, toluene and O₃ would directly react on the surface of the catalyst so that O₃ could be consumed; on the other hand, toluene would react with the precursor that generated ozone on the surface of the catalyst, which indirectly led to a decrease in ozone content. However, the output of ozone decreased slightly after adding toluene to the reactor because the by-products generated during the reaction covered the active sites on the surface of the catalyst carrier, reducing the catalytic activity of γ -Al₂O₃. At the same time, these byproducts occupied the active sites on the surface of the catalyst, preventing toluene from reacting with the active oxygen groups on the surface.

The O₃ concentration in the reactor loaded with TiO₂/ γ -Al₂O₃ was higher than that in the reactor loaded with blank γ -Al₂O₃. TiO₂ could be excited to generate hole–electron pairs under the action of DBD, and the holes had a strong oxidizing ability;

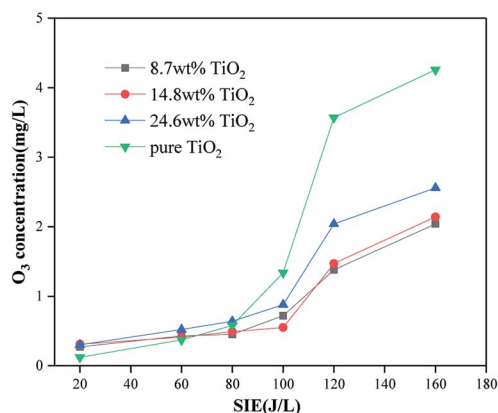


Fig. 13 Ozone concentrations of different TiO₂ catalytic reactors.

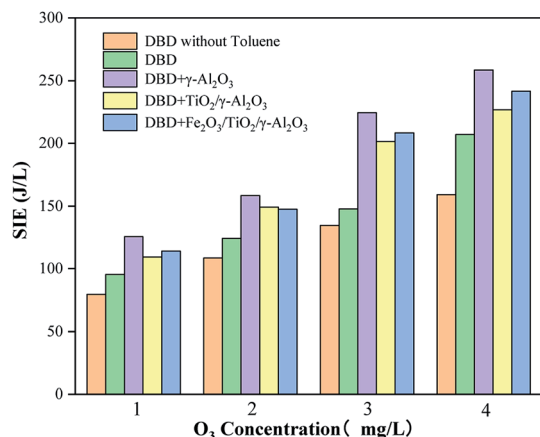


Fig. 14 SIE under different ozone production levels.

meanwhile, a large amount of O₃ was generated, and the O₃ would also be decomposed on the surface of the catalyst during the reaction process.³⁰

In addition, it can be seen from Fig. 11 that the concentration of ozone was lower in the reactors loaded with Fe₂O₃/TiO₂/γ-Al₂O₃ and TiO₂/γ-Al₂O₃ than in the DBD reactor. The concentration of ozone in the former reactor was the lowest.

This showed that the addition of Fe₂O₃ not only consumed the oxygen used to generate ozone but also promoted the decomposition of ozone or make ozone form active groups to participate in the degradation reaction and further reduce the concentration of ozone. The concentrations of ozone produced by the two catalytic reactors were not much different. The O₃ concentration produced by the reactor loaded with Fe₂O₃/TiO₂/γ-Al₂O₃ was lower than that in the reactor loaded with TiO₂/γ-Al₂O₃. This result was in agreement with the previous removal rate comparison, which further showed that the Fe₂O₃/TiO₂/γ-Al₂O₃ catalyst has higher catalytic activity.

Four catalytic reactors were prepared by loading TiO₂ on γ-Al₂O₃ and directly coating TiO₂ on the electrode. The removal efficiency of toluene and the output of O₃ were evaluated under different SIE values. It can be seen from Fig. 12 and 13 that with the help of the γ-Al₂O₃ carrier, the TiO₂ carried on the γ-Al₂O₃ carrier showed a higher toluene removal efficiency and a lower O₃ output than pure TiO₂. This is because more pollutant molecules will be adsorbed onto the surface of the catalyst, which increases the probability of reacting with active substances on the catalyst surface. After TiO₂ is excited, the carrier facilitates the exposure of pollutant molecules to the generated holes. As shown in Fig. 12, reactors with different TiO₂ wt% show similar treatment efficiencies and ozone

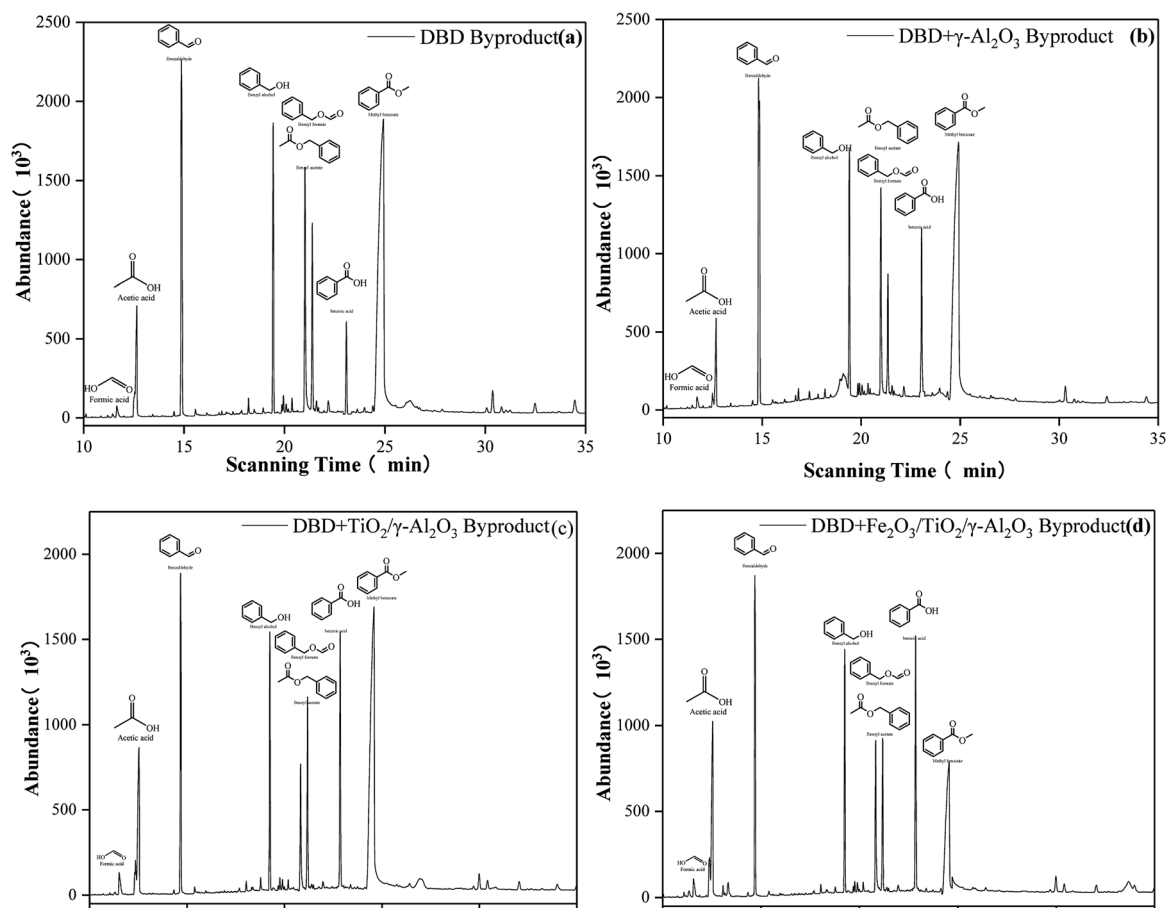


Fig. 15 Byproducts generated in DBD (a), DBD + γ-Al₂O₃ (b), DBD + TiO₂/γ-Al₂O₃ (c), DBD + Fe₂O₃/TiO₂/γ-Al₂O₃ (d).



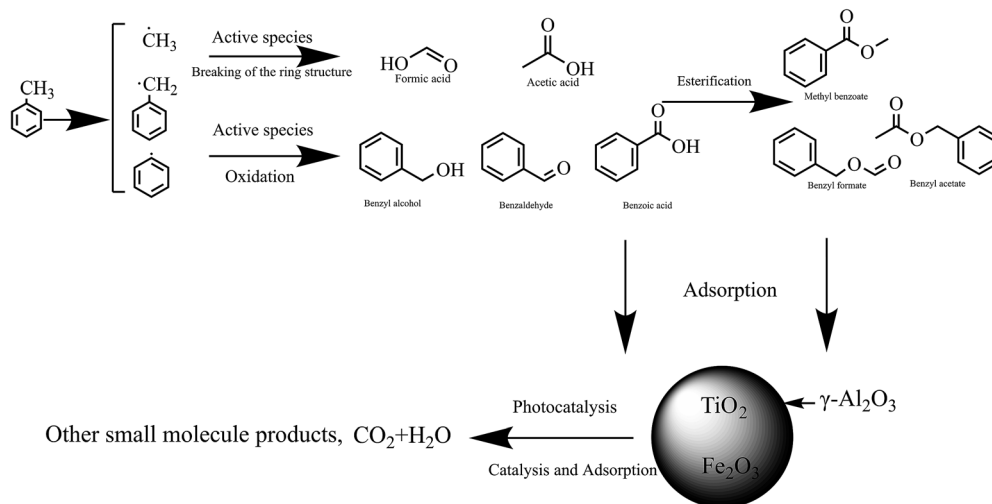


Fig. 16 Reaction mechanism.

production. Among these, the catalytic reactor with about 15 wt% TiO_2 has the best effect. This is because a suitable weight percentage of TiO_2 can not only generate enough electron-hole pairs to oxidize pollutant molecules, but will also not cover too many catalyst sites, thereby affecting the adsorption effect of the pollutant molecules. Pure TiO_2 shows lower processing efficiency and higher ozone production. This is because the lack of catalyst carrier adsorption of pollutant gas molecules reduces the residence time of gas molecules in the reactor and is not conducive to the consumption of ozone on the surface of the catalyst. Through control experiments on the amount of ozone produced by different reactors under different SIE values, the research showed that under different O_3 concentration levels, the reactor loaded with Al_2O_3 has the highest SIE value; the SIE values of the reactors loaded with $\text{TiO}_2/\gamma\text{-Al}_2\text{O}_3$ and $\text{Fe}_2\text{O}_3/\text{TiO}_2/\gamma\text{-Al}_2\text{O}_3$ are slightly lower, indicating that the Al_2O_3 catalyst has the best controlling effect on ozone, and the results are also consistent with the research of ozone production under the same SIE (Fig. 14).

Byproduct analysis

Active groups containing oxygen and nitrogen were formed during the discharge process after toluene and background gas molecules (N_2 and O_2) entered the reactor. These active groups and the high-energy electrons generated by the discharge would react with the toluene molecules to form a large amount of intermediate product. The chemical bonds with low bond energy in the toluene molecule would be destroyed by the particles, active groups with relatively low energy and some chemical bonds with higher bond energy, such as benzene rings, in this process. The energy would also be reduced during the collision with the particles, resulting in preliminary purification of the toluene molecules.

As shown in Fig. 15(b), $\gamma\text{-Al}_2\text{O}_3$ had the function of adsorbing organic gas molecules, prolonging their residence time in the DBD process, and increasing the probability of collisions between high-energy electrons generated in the DBD process and gas molecules; this facilitates the production of high-energy

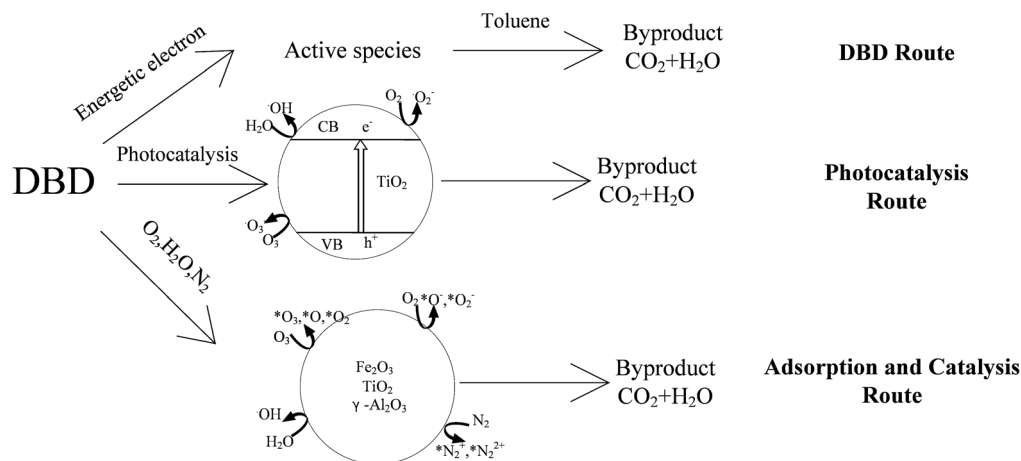


Fig. 17 Mechanism of co-processing.

Table 1 Effects of different catalyst discharge length ratios on toluene treatment

Discharge length ratio (Fe ₂ O ₃ /TiO ₂ /γ-Al ₂ O ₃ : TiO ₂ / γ-Al ₂ O ₃ : γ-Al ₂ O ₃)	Value of SIE when the highest removal efficiency is reached (J L ⁻¹)	Selectivity of CO ₂ when the highest removal efficiency is reached (%)	O ₃ concentration when the highest removal efficiency is reached (mg m ⁻³)	NO _x concentration when the highest removal efficiency is reached (mg m ⁻³)
1 : 1 : 1	207.8	58.87	2260	131.58
1 : 1 : 2	216.9	59.52	2010	128.56
1 : 2 : 1	189.7	69.32	2450	130.42
1 : 2 : 2	183.4	67.74	2180	117.66
2 : 1 : 1	205.8	42.31	3130	141.87
2 : 1 : 2	218.6	49.58	2790	127.41
2 : 2 : 1	210.1	54.56	3740	147.69

particles or strong oxidizing properties, promoting the decomposition of the organic gas.

After TiO₂ was loaded on γ-Al₂O₃, the concentrations of benzyl formate, benzaldehyde and benzyl alcohol were significantly reduced. At the same time, the concentrations of benzoic acid, formic acid, and acetic acid increased, which can be found in Fig. 15(c). The results showed that the combination of photocatalysis and DBD strengthened the degradation ability of toluene molecules, which was beneficial to further improvement of the selectivity of CO₂.

When Fe₂O₃/TiO₂/γ-Al₂O₃ was added to the DBD reactor, a large number of active groups and high-energy particles generated by the DBD process and catalytic reaction were adsorbed on the surface of the catalyst carrier, and a series of reactions occurred on the active sites of the catalyst which further improved the decomposition rate of the organic mixture. It can be seen from Fig. 15(d) that the addition of Fe₂O₃ further reduced the concentration of methyl benzoate. More small molecules appeared under the synergistic effect of the photocatalysis and DBD reaction, which showed that the addition of Fe₂O₃ promoted the decomposition of toluene and intermediate products, pushing the reaction forward in the direction of producing smaller molecules. The inferred reaction mechanism is shown in Fig. 16 and 17.

Synergistic effects of different catalysts

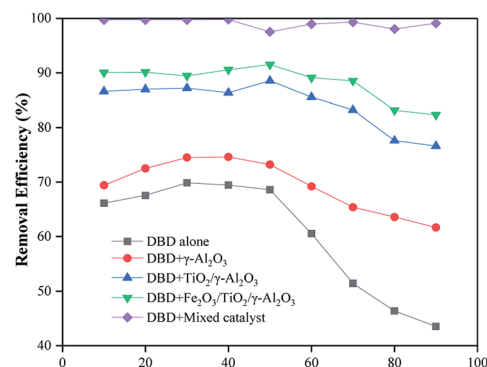
From the research above, it can be found that different catalysts have their own advantages and disadvantages when cooperating with DBD to treat toluene. Therefore, this study considered the location of different catalysts in the DBD reactor according to the processing characteristics to maximize the removal efficiency and selectivity of CO₂ and reduce the generation of by-products. Compared with other catalysts, Fe₂O₃/TiO₂/γ-Al₂O₃ had higher treatment efficiency and selectivity of CO₂. Therefore, Fe₂O₃/TiO₂/γ-Al₂O₃ was used as the catalyst in the first section to degrade part of the toluene and promote the reaction in the direction of generating more small molecules. However, it can be seen from Fig. 15 that the DBD process using Fe₂O₃/TiO₂/γ-Al₂O₃ as a catalyst would produce more kinds of by-products. The synergy of γ-Al₂O₃ loaded with TiO₂ and DBD could further reduce the output of by-products, especially for the removal of small molecule products. Therefore, this study considered using TiO₂ as the catalyst in the second section to

oxidize small molecules and continue to degrade toluene.³¹ The combination of DBD and γ-Al₂O₃ achieved the lowest concentration of ozone and NO_x in the experiment; therefore, γ-Al₂O₃ was considered as the third-stage catalyst to decompose ozone and NO_x in order to increase the selectivity of CO₂ and reduce the by-product concentration. After determining the types of catalysts in the different discharge regions, the discharge lengths occupied by different catalysts were compared. The research results showed that the removal efficiency could reach more than 99.7% under a certain value of SIE (Table 1).

The results showed that the reactor with a discharge length ratio of 1 : 2 : 2 only needed 183.4 J L⁻¹ of SIE when the removal efficiency reached the highest level, and the selectivity of CO₂ was slightly lower than that of 1 : 2 : 1 because the catalytic activity of γ-Al₂O₃ was lower than those of the other two, resulting in a decrease in the selectivity of CO₂. At the same time, the O₃ and NO_x concentrations in this type of reactor were lower than in the other kinds of reactors when it reached the highest treatment efficiency. Compared with the Fe₂O₃/TiO₂/γ-Al₂O₃-DBD reactor, the reactor with a discharge length ratio of 1 : 2 : 2 achieved 21.16% increased selectivity of CO₂, the O₃ output decreased by 26.9%, and the NO_x content decreased by 9.1%.

Effects of humidity on the processing efficiency

By comparing the toluene removal efficiencies of different reactors under different humidity levels, it could be found that the reactor loaded with γ-Al₂O₃ and the single DBD reactor

**Fig. 18** The relationships between humidity and removal efficiency in different types of DBD reactors.

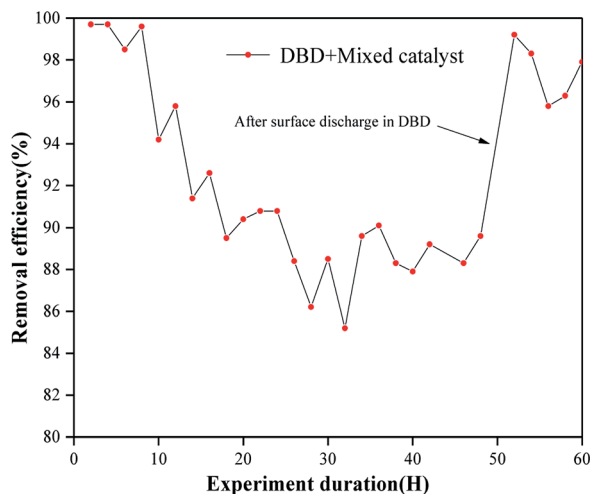


Fig. 19 Long term experiment of removal efficiency.

showed a small increase when the humidity was 10–30% because H_2O was decomposed into hydroxyl radicals in the DBD process to promote the decomposition of toluene molecules under an SIE of 200 J L^{-1} . When the humidity was 30–90%, there was a sharp drop because too many H_2O molecules could not undergo timely decomposition, which reduced the electron density and accelerated the demise of free radicals. At the same time, the presence of H_2O molecules would compete with other groups to adsorb on the catalyst surface, reducing the number of active sites for toluene and O_3 adsorption.³² The reactor loaded with TiO_2 and Fe_2O_3 catalysts was less affected by humidity than the first two reactors, which proved that these two catalysts could break down more water molecules and had stronger catalytic activity (Fig. 18).

Regeneration of catalyst

The research showed that after 48 hours of reaction, due to the accumulation of by-products on the surface of the catalyst, the

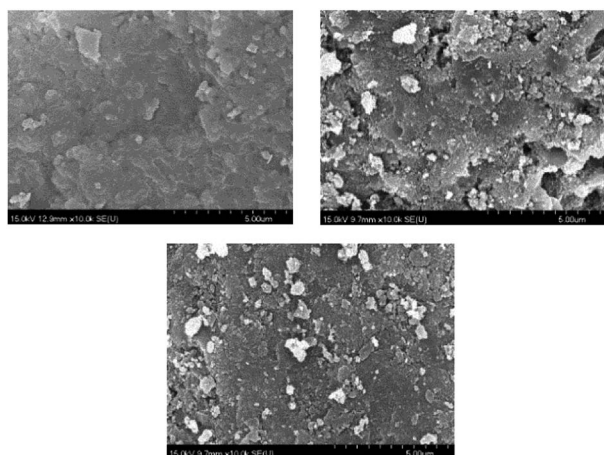


Fig. 20 SEM patterns of regenerated $\gamma\text{-Al}_2\text{O}_3$, $\text{TiO}_2/\gamma\text{-Al}_2\text{O}_3$ and $\text{Fe}_2\text{O}_3/\text{TiO}_2/\gamma\text{-Al}_2\text{O}_3$.



Fig. 21 Photograph of $\text{Fe}_2\text{O}_3/\text{TiO}_2/\gamma\text{-Al}_2\text{O}_3$ before use (1), after use (2), and after regeneration (Re).

carbon deposits produced gradually reduced the efficiency of the catalyst, and the treatment efficiency eventually dropped to about 88.6%. After 48 hours of use, there were carbon deposits on the surface; then, the different types of catalysts were placed in a DBD environment for surface discharge treatment for 2 hours. After surface discharge, it can be seen from Fig. 21 that the carbon deposits on the surface basically disappeared. From the SEM image (Fig. 20), it can be found that the small particles on the surface of the mixed catalyst still exist, and there is no obvious change in particle size; however, it can be seen from Fig. 20 that the surface of the catalyst became slightly rough and uneven, possibly due to corrosion by carbon deposits. The mixed catalyst was placed into the DBD reactor, and the test of the removal rate of toluene was continued. As shown in Fig. 19, the removal efficiency was basically restored.

Conclusions

This study compared the removal rates, mineralization rates, SIE values and by-product outputs of different catalysts when synergizing DBD to treat toluene. Based on the value of SIE, the advantages and disadvantages of different catalysts to remove toluene were considered, and a mixed-catalyst synergistic DBD reaction was designed. Compared with the single catalyst and DBD treatment of toluene, a removal rate of more than 99.7% and CO_2 selectivity of 67.74% were achieved under the conditions of an $\text{Fe}_2\text{O}_3/\text{TiO}_2/\gamma\text{-Al}_2\text{O}_3 : \text{TiO}_2/\gamma\text{-Al}_2\text{O}_3 : \gamma\text{-Al}_2\text{O}_3$ discharge length ratio of 1 : 2 : 2 and an SIE value of 183.4 J L^{-1} , while the concentrations of O_3 and NO_x were reduced as well. In addition, the reactor in which the multiple catalysts worked together was stable under different humidity conditions, which indicates that this kind of reactor has the potential to remove toluene in a complex ambience.

Conflicts of interest

There are no conflicts to declare.

Acknowledgements

This work was financially supported by the Anhui Provincial Science and Technology Major Special Project (17030801034).



Notes and references

- 1 K. Barbusinski, K. Kalembe, D. Kasperczyk, K. Urbaniec and V. Kozik, *J. Clean. Prod.*, 2017, **152**, 223–241.
- 2 B. Belaisaoui, Y. Le Moullec and E. Favre, *Energy*, 2016, **95**, 291–302.
- 3 R. Hariz, J. I. del Rio Sanz, C. Mercier, R. Valentin, N. Dietrich, Z. Mouloungui and G. Hébrard, *Chem. Eng. Sci.*, 2017, **157**, 264–271.
- 4 C. Qin, X. Huang, J. Zhao, J. Huang, Z. Kang and X. Dang, *J. Hazard. Mater.*, 2017, **334**, 29–38.
- 5 W. Yang, H. Zhou, C. Zong, Y. Li and W. Jin, *Sep. Purif. Technol.*, 2018, **200**, 273–283.
- 6 B. Chen, L. Wu, B. Wu, Z. Wang, L. Yu, M. Crocker, A. Zhu and C. Shi, *ChemCatChem*, 2019, **11**, 3646–3661.
- 7 Y. Liu, L. Lian, W. Zhao, R. Zhang and H. Hou, *Plasma Sci. Technol.*, 2020, **22**, 034016.
- 8 L. Zhou, C. Ma, J. Horlyck, R. Liu and J. Yun, *Catalysts*, 2020, **10**, 668–717.
- 9 H. Yu, W. Hu, J. He and Z. Ye, *Chemosphere*, 2019, **237**, 124439.
- 10 K. L. Pan and M. B. Chang, *Environ. Sci. Pollut. Res. Int.*, 2019, **26**, 12948–12962.
- 11 A. H. Khoja, M. Tahir and N. A. S. Amin, *Energy Convers. Manage.*, 2019, **183**, 529–560.
- 12 S. K. P. Veerapandian, N. De Geyter, J.-M. Giraudon, J.-F. Lamonier and R. Morent, *Catalysts*, 2019, **9**, 98–138.
- 13 L. Guo, N. Jiang, J. Li, K. Shang, N. Lu and Y. Wu, *Front. Environ. Sci. Eng.*, 2018, **12**, 15.
- 14 M. F. Mustafa, X. Fu, Y. Liu, Y. Abbas, H. Wang and W. Lu, *J. Hazard. Mater.*, 2018, **347**, 317–324.
- 15 C. Norsic, J.-M. Tatibouët, C. Batiot-Dupeyrat and E. Fourré, *Chem. Eng. J.*, 2018, **347**, 944–952.
- 16 B. Wang, B. Chen, Y. Sun, H. Xiao, X. Xu, M. Fu, J. Wu, L. Chen and D. Ye, *Appl. Catal. B Environ.*, 2018, **238**, 328–338.
- 17 B. Wang, C. Chi, M. Xu, C. Wang and D. Meng, *Chem. Eng. J.*, 2017, **322**, 679–692.
- 18 X. Zhang, G. Zhang, Y. Wu and S. Song, *AIP Adv.*, 2018, **8**, 125109.
- 19 X. Zhu, X. Gao, R. Qin, Y. Zeng, R. Qu, C. Zheng and X. Tu, *Appl. Catal. B Environ.*, 2015, **170–171**, 293–300.
- 20 X. Zhu, S. Liu, Y. Cai, X. Gao, J. Zhou, C. Zheng and X. Tu, *Appl. Catal. B Environ.*, 2016, **183**, 124–132.
- 21 B. Zhu, L.-Y. Zhang, M. Li, Y. Yan, X.-M. Zhang and Y.-M. Zhu, *Chem. Eng. J.*, 2020, **381**, 122599.
- 22 N. Jiang, Y. Zhao, K. Shang, N. Lu, J. Li and Y. Wu, *J. Hazard. Mater.*, 2020, **393**, 122365.
- 23 S. Li, X. Dang, X. Yu, G. Abbas, Q. Zhang and L. Cao, *Chem. Eng. J.*, 2020, **388**, 124275.
- 24 A. P. Roberts, Q. Liu, C. J. Rowan, L. Chang, C. Carvallo, J. Torrent and C.-S. Horng, *J. Geophys. Res.: Solid Earth*, 2006, **111**, 35–51.
- 25 E. Y. Mora, A. Sarmiento, E. Vera, V. Drozd, A. Durigyn and S. Saxena, *J. Phys.: Conf. Ser.*, 2017, **935**, 012044.
- 26 J. Ma, C. Zhu, J. Lu, H. Liu, L. Huang, T. Chen and D. Chen, *Solid State Sci.*, 2015, **49**, 1–9.
- 27 J. Chen, X. Chen, W. Xu, Z. Xu, J. Chen, H. Jia and J. Chen, *Chem. Eng. J.*, 2017, **330**, 281–293.
- 28 W. Liang, H. Sun, X. Shi and Y. Zhu, *Catalysts*, 2020, **10**, 511.
- 29 X. Zhao, X. Liu, J. Liu, J. Chen, S. Fu and F. Zhong, *J. Phys. D: Appl. Phys.*, 2019, **52**, 145201.
- 30 X. Yao, J. Zhang, X. Liang and C. Long, *Chemosphere*, 2019, **230**, 479–487.
- 31 B. Zhu, L. Zhang, Y. Yan, M. Li and Y. Zhu, *Plasma Sci. Technol.*, 2019, **21**, 115503.
- 32 S. Li, X. Dang, X. Yu, R. Yu, G. Abbas and Q. Zhang, *J. Hazard. Mater.*, 2020, **400**, 123259.

